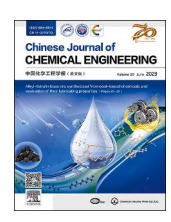
FISEVIER

Contents lists available at ScienceDirect

Chinese Journal of Chemical Engineering

journal homepage: www.elsevier.com/locate/CJChE



Full Length Article

Physicochemical properties of UO₃ products synthesized *via* a flame denitrification reactor



Jiaxin Liu ^{1, #}, Mingming Wu ^{2, #}, Qichao Li ¹, Rui Li ¹, Lei Li ¹, Liudong Hou ^{1, *}, Yi Liu ^{2, *}, Jing Ma ^{1, *}

- ¹ China Nuclear Power Engineering Co., Ltd., Beijing 100142, China
- ² School of Chemical Engineering, Dalian University of Technology, Dalian 116024, China

ARTICLE INFO

Article history:
Received 29 March 2025
Received in revised form
21 May 2025
Accepted 11 June 2025
Available online 8 August 2025

Keywords: Flame denitrification reactor Uranium trioxide synthesis Nuclear fuel cycle Chemical processes Thermodynamics

ABSTRACT

The rational utilization of nuclear energy is crucial in current global energy system. Using a flame denitrification reactor, this study develops uranium trioxide (UO₃), a critical intermediate product in the nuclear fuel cycle, and systematically characterizes its physicochemical properties. The UO₃ products are comprehensively examined to assess their suitability for downstream nuclear industry applications. Our results indicates that high-quality UO₃ products can be obtained using flame denitrification reactor at temperatures between 440°C and 480 °C. This study reveals the considerable potential of UO₃ production *via* flame denitrification, marking a significant advancement towards enhanced nuclear fuel cycle systems.

© 2025 The Chemical Industry and Engineering Society of China, and Chemical Industry Press Co., Ltd. All rights are reserved, including those for text and data mining, Al training, and similar technologies.

1. Introduction

The development and utilization of nuclear energy are essential for addressing global concerns regarding energy shortage, energy structure optimization, and carbon emission reduction [1–4]. Nuclear power generation mitigates global warming and ensures sustainable energy supply. Uranium (U), a critical nuclear fuel for reactors, requires efficient oxide production to support the nuclear industry [5–9]. In nuclear fuel cycle systems, UO₃ serves as both the starting material for uranium enrichment [10–12] and the uranium product for plutonium enrichment [13–15]. Uranyl nitrate thermally decomposes to yield uranium oxides. This process is commonly conducted using fluidized bed reactors [16] or flame denitrification reactors [17]. Fluidized bed reactors can achieve denitrification by atomizing uranyl nitrate solution into small droplets, which are then sprayed into a fluidized bed using compressed air. The fluidized bed sustains continuous fluidization and

This article is part of a special issue entitled: 100th Anniversary of SCET, TJU published in Chinese Journal of Chemical Engineering.

E-mail addresses: hould@cnpe.cc (L. Hou), diligenliu@dlut.edu.cn (Y. Liu), majing@cnpe.cc (J. Ma).

heating of uranium oxide particles. Uranyl nitrate droplets sprayed onto the bed undergo dehydration and decomposition into uranium oxide, followed by discharge through an outlet. Flame denitrification reactors generate high-temperature gas in a burner through combining methane, propane, butane, or similar gases with combustion-supporting air. The uranyl nitrate feed undergoes denitrification upon contacting high-temperature gas within a vertical reactor. Uranium oxide is commonly prepared via dehydration and thermal decomposition. Fluidized bed reactors feature long residence durations, which are unsuitable for largescale uranyl nitrate treatment, owing to nuclear critical risk. For instance, the diameter of the reaction zone does not exceed 420 mm in a fluidized bed reactor with a ²³⁵U enrichment of 1.5%, limiting the processing capacity up to 2.5 $t \cdot d^{-1}$ [18–20]. In contrast, flame denitrification reactors, designed for highthroughput uranyl nitrate treatment, exhibit remarkably reduced residence durations.

In addition, the fluidized bed reactor relies on electric heating for reaction temperature control, resulting in high energy consumption. In contrast, flame denitrification reactors utilize inexpensive gaseous fuels to provide reaction energy, thereby making the production process more economical. Nonetheless, the use of flame denitrification reactors to produce UO₃ remains largely unexplored. To address this concern, in this study, we pioneered

^{*} Corresponding authors.

^{*} These authors contributed equally to this work.

the preparation of UO₃ using a flame denitrification reactor. The effect of combustion conditions on the UO₃ production process was investigated in detail, and obtained UO₃ products were systematically studied to assess its suitability for downstream hydrogenation reduction and hydro-fluorination processes.

2. Experimental

2.1. Materials

All the reagents (Liquefied petroleum gas, combustion air, uranyl nitrate, nitric acid) used for the experiments were obtained from CNU 272 Uranium Industrial Co., Ltd.

2.2. Sample characterization

The morphology of samples was characterized by scanning electron microscopy (SEM, Hitachi FlexSEM 1000) at accelerating voltages of 5–15 kV.

Thermogravimetric analysis (TGA) was tested by TG 209 (NETZSCH) under air purge in a temperature range between 40 and 800 $^{\circ}$ C at ramping rate of 10 $^{\circ}$ C · min $^{-1}$.

The X-ray diffraction (XRD; Rigaku D/MAX-RB) patterns of samples were recorded at 100 mA and 40 kV in the 2θ range of $5^{\circ}-90^{\circ}$ using monochromatised Cu K_{α} radiation and a scan rate of $10^{\circ}\cdot min^{-1}$.

The temperature-programmed reduction (TPR) of samples was conducted using a chemisorption analyser (AutoChemII2920). Prior to assessment, the sample (~50 mg) was dehydrated in the isothermal region of a quartz U-tube reactor at 400 °C for 2 h in a

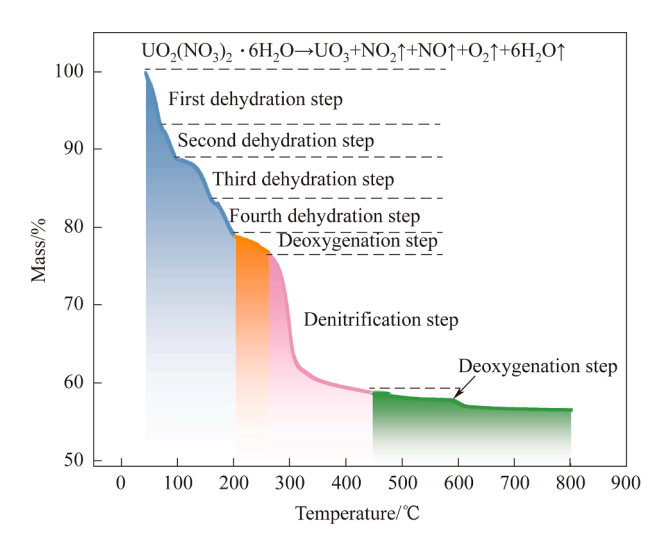


Fig. 1. Thermogravimetric analysis of uranyl nitrate.

flow of He (30 ml·min $^{-1}$) to eliminate physisorbed water. Then the sample was cooled to room temperature, and TPR curves were recorded in a flow of 10% H $_2$ /He (30 ml·min $^{-1}$) as the temperature was linearly increased to 800 °C at heating rate of 5 °C·min $^{-1}$.

Fourier transform infrared attenuated total reflection spectra (ATR-FTIR), using a Thermo Fisher iN10 spectrometer equipped with a liquid-nitrogen-cooled MCT detector, were recorded within the spectral range of $650-4000\,\mathrm{cm}^{-1}$ with a resolution of $4\,\mathrm{cm}^{-1}$ and $16\,\mathrm{scans}$ for signal accumulation.

The X-ray photoelectron spectroscopy (XPS) was executed employing a photoelectron spectrometer (ESCALAB250) supplemented with a monochromatic source of Al $\rm K_{\alpha}$ X-ray (1486.6 eV), exerted at 20 mA and 15 kV. The pretreatment of samples was carried out under situ conditions (200 °C for 2 h under a 40 ml·min $^{-1}$ Ar flow) and subsequently placed into a rigid vacuum typically in the range of less than 3.5×10^{-7} Pa. The adventitious peak of carbon (C 1s) at 284.6 eV was considered as the internal reference. The chemical state was evaluated through the peaks areas from the curve fitting of the regions of U 4f employing the XPSPEAK computer program.

2.3. Flame denitrification

The uranyl nitrate solution (1000 g·L⁻¹, 0.05 m³·h⁻¹, the concentration of nitric acid is 1 mol L^{-1}) is sourced from the existing concentrated denitration plant within the factory premises (CNU 272 Uranium Industrial Co., Ltd.), and is quantitatively transported by the uranium solution feeding metering pump to the flame denitrification reactor (Fig. S1, Supplementary Material) for the denitration process. The uranyl nitrate solution is introduced into the reaction chamber through an air-liquid dual-phase atomizing nozzle positioned at the center of the burner at the top of the flame denitrification reactor. The heat generated by the combustion of liquefied petroleum gas (LPG) is utilized to drive the denitration pyrolysis reaction of the uranyl nitrate solution, resulting in the formation of UO₃ solid particles. The UO₃ product is conveyed to the storage silo through a discharge valve and subsequently transferred into uranium product barrels. The LPG is supplied by the liquefied petroleum gas (LPG) supply system.

After emerging from the atomizing gas stabilization tank, compressed air at 0.4 MPa is directed into the atomizing gas heater, where it is heated to 250 °C before being delivered to the dual-fluid atomizing nozzle positioned at the top of the flame denitrification reactor. An electric heater is installed along the atomizing gas intake pipeline to ensure optimal temperature control. Meanwhile, combustion-supporting air, either sourced from the stabilization tank or pressurized by the booster fan, is heated to 400 °C *via* the combustion air heater before being conveyed to the burner's combustion-supporting air inlet at the reactor's top. Liquefied petroleum gas (LPG), after undergoing pressure reduction and vaporization, is then supplied to the burner inlet at the top of the flame denitrification reactor.

Table 1	
Performance of LIO ₂ at different reaction chamber temperatures	

Propane flow	Combustion-supporting air flow $/L \cdot h^{-1}$	Reaction chamber temperature /°C	Analysis of UO ₃ products			
rate/L·h ^{−1}			Uranium mass fraction/%	Specific surface area/m ² ·g ⁻¹	Nitrate mass fraction/%	H ₂ O mass fraction/%
0.92	77.00	400	80.3	4.74	1.8	1.4
1.05	90.00	440	81.0	11.07	1.5	0.8
1.29	125.00	480	81.9	12.10	0.6	0.6
1.41	135.00	520	82.2	12.80	0.5	0.3

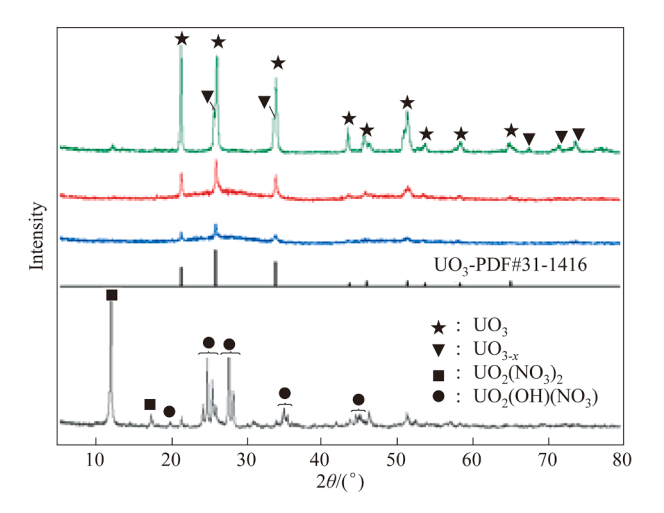


Fig. 2. XRD patterns of the thermal decomposition products of uranyl nitrate. (Green: UO_3 -520; Red: UO_3 -480; Blue: UO_3 -440; Black: UO_3 -400).

3. Results and Discussion

To determine the optimal decomposition temperature and elucidate the decomposition mechanism of uranyl nitrate, thermogravimetric analysis is first conducted to identify the decomposition pathway of uranyl nitrate precursor (Fig. 1). The

thermogravimetric curve in Fig. 1 reveals six distinct mass loss stages. The minor weight observed in the sixth stage suggests that UO₃ undergoes complete thermal decomposition at ~595 °C. At 200 °C, the sample exhibits a mass loss of 20.9%, which is consistent with the content of water molecules in uranyl nitrate (21.5%, mass). Therefore, primary dehydration occurs below 200 °C, encompassing the first four continuous dehydration steps. Specifically, the first dehydration step occurs between 0 °C and 68 °C with a mass loss of 7.3%, corresponding to the removal of 2 mol H₂O. The second dehydration step occurs between 69 °C and 95 °C with a mass loss of 3.6%, corresponding to the removal of 1 mol H₂O. The third dehydration step occurs between 96°C and 158 °C with a mass loss of 5.5%, corresponding to the removal of 1.5 mol H₂O. The fourth dehydration step occurs between 159 °C and 200 °C with a weight loss of 4.5%, corresponding to the removal of the final 1.25 mol H₂O. Therefore, the tetrahydrate and trihydrate forms of uranyl nitrate are formed at 68°C and 95 °C, respectively.

Notably, the remaining 3 mol $\rm H_2O$ is not removed between $\rm 96^{\circ}C$ and 200 °C, confirming that the dehydration of the 6 mol $\rm H_2O$ is not complete until increasing to above 200 °C. This can be attributed to the accumulation of water vapor around the hydrate particles during dehydration and hydrolysis of uranyl nitrate. Dehydration intermediates (or intermediate hydrates) are stable in multinuclear environments and mainly exist as entities either separated from crystallized water molecules or coordinated with hydroxyl groups. The properties and stoichiometry of hydroxyuranyl nitrate depend on the degree of hydrolysis, which is

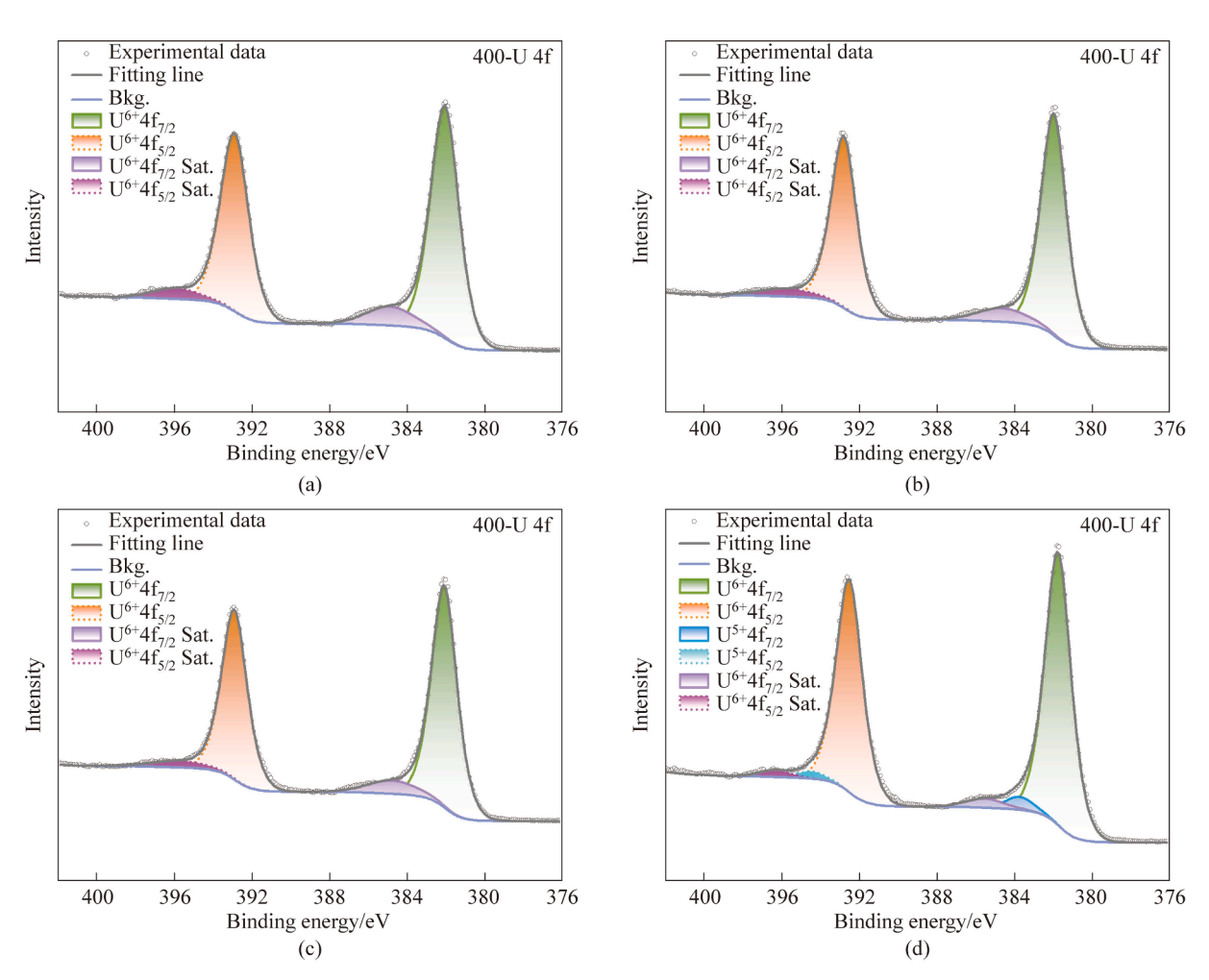


Fig. 3. X-ray photoelectron spectra of the UO_3 samples. (a) UO_3 -400, (b) UO_3 -440, (c) UO_3 -480, and (d) UO_3 -520.

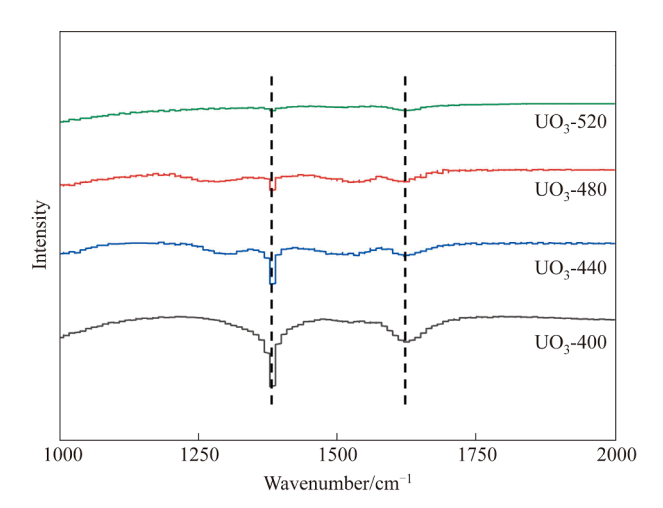


Fig. 4. Fourier-transform infrared (FTIR) spectra of the UO₃ samples.

influenced by the amount of water vapor surrounding the sample particles and residence time [21].

Following the dehydration stage, our sample undergoes a significant mass loss of ~19% (mass). In addition to dehydration, nitrogen oxides are removed. The observed mass loss matches well with the theoretical value for the removal of 0.25 mol H_2O , 1 mol NO, 1 mol NO_2 , and 0.5 mol O_2 , accounting for 19.2% of the initial

amount of uranyl nitrate (molar mass of 502). In addition, our sample exhibits a mass loss of 3.1% (mass) between 200 °C and 267 °C, corresponding to the removal of ~0.5 mol O_2 . At 268–440 °C, the sample exhibits rapid mass loss, attributed to the removal of NO, NO₂, and residual water.

After the denitrification step, a mass loss of ~1% is observed at ~600 °C, which is consistent with the conversion of UO_3 to U_3O_8 (1.00% (mass)) in the final stage of uranyl nitrate decomposition. The subsequent thermogravimetric curve shows a slight fluctuation due to the presence of U_3O_8 , which often exists as non-stoichiometric U_3O_{8-x} , where x is associated with both temperature and oxygen partial pressure. At higher temperatures, oxygen escapes from the lattice; simultaneously, the resulting vacancy is replenished with oxygen from the surrounding gaseous environment. It should be noted that the variation in temperature could lead to different crystal forms of U_3O_8 with distinct density values, causing a slight fluctuation in the thermogravimetric curve at temperature above 600 °C.

Therefore, the flame denitrification reaction requires a minimum operation temperature of 300 °C. At 300 °C, the obtained product appears yellow-green, indicating incomplete uranyl nitrate decomposition. This could be attributed to the insufficient reaction caused by the lower temperature. Based on the above results, the reaction temperature is increased to 440–520 °C.

To investigate the relationship between product performance and operation conditions, the thermal decomposition behavior of uranyl nitrate is further assessed using a flame denitrification reactor. The reaction temperature is accurately controlled by

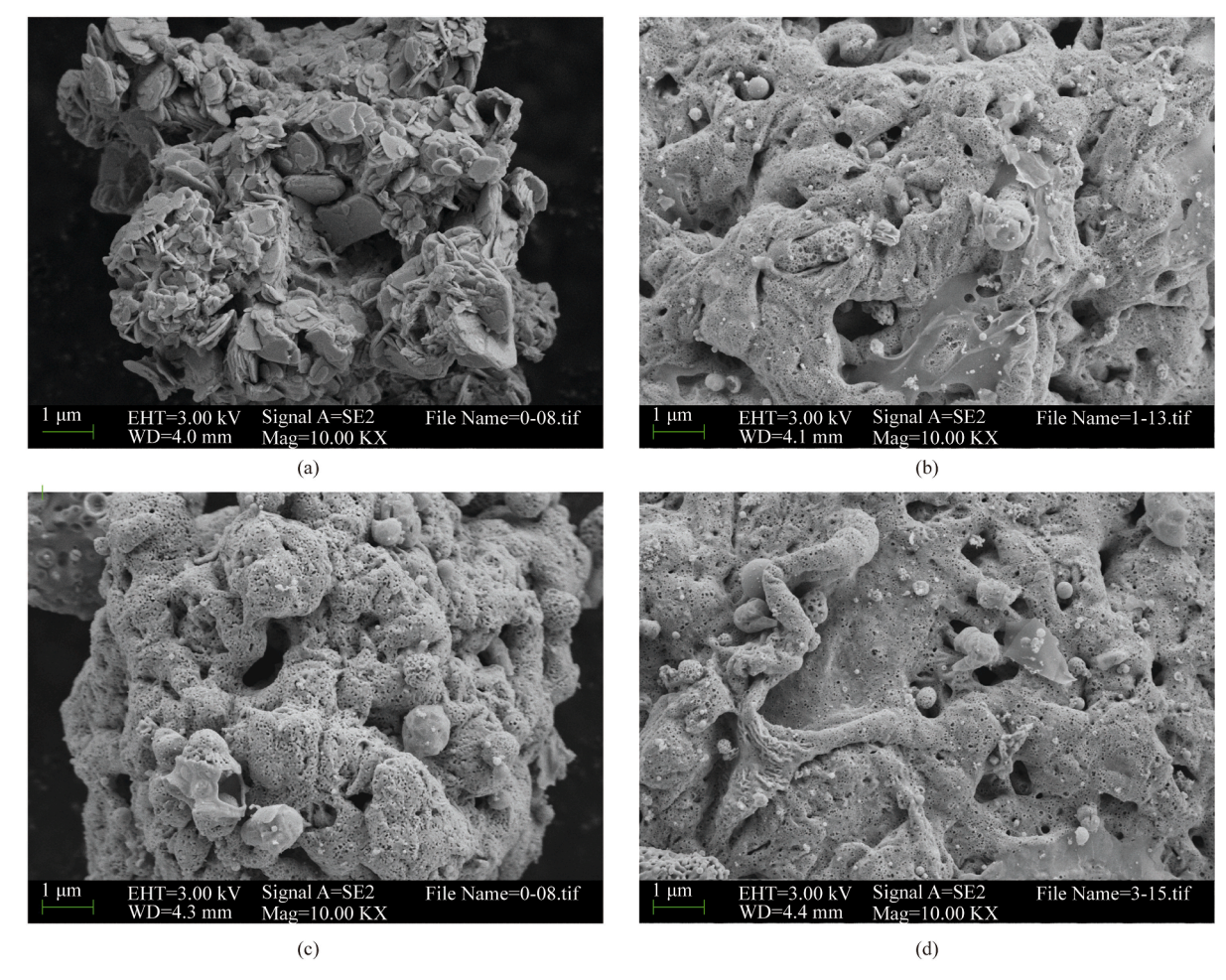


Fig. 5. Scanning electron microscopy (SEM) images of the UO₃ samples: (a) UO₃-400, (b) UO₃-440, (c) UO₃-480, and (d) UO₃-520.

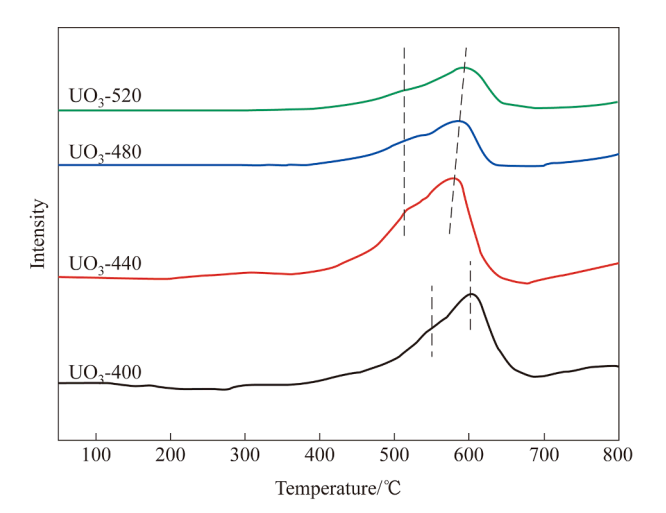


Fig. 6. H₂-TPR curves of the UO₃ samples.

adjusting the combustion chamber temperature and flow rates of the liquefied combustion-supporting air and propane. Four representative reaction conditions are selected to obtain four groups of samples (UO₃-400, UO₃-440, UO₃-480, and UO₃-520), and their textural properties, including particle size, specific surface area, NO₃ content, water content, and total uranium mass fraction, are investigated in detail. Corresponding results are summarized in Table 1.

At 400 °C, obtained product exhibiting low specific surface area contains ~1.8% (mass) uranyl nitrate and 1.4% (mass) water, which fails to meet the subsequent requirement on uranium enrichment or postprocessing to produce $MO_{\rm x}$ fuel. At 450 °C, the conversion rate and water content of the product are improved, indicating that thermal decomposition of uranyl nitrate using the flame denitrification reactor is sensitive to the reaction temperature. Since the mass fraction of UO_3 in the product is calculated according to the mass fraction of U, further physicochemical characterization is conducted to verify whether the deoxidation product U_3O_8 is formed in excess.

Fig. 2 illustrates X-ray diffraction (XRD) patterns of four sample groups. XRD peaks in the spectrum of UO₃-400 are miscellaneous, indicating an incomplete flame denitrification reaction at 400 °C due to insufficient residence time. The yellow-green block is likely a mixture of $UO_2(OH)(NO_3) \cdot 3H_2O$, $UO_2(NO_3)_2 \cdot 3H_2O$, $UO_2(OH)(NO_3) \cdot H_2O$, and $UO_2(NO_3)_2 \cdot xH_2O$ (x < 6). At temperature exceeding 440 °C, relevant XRD patterns of obtained products show diffraction peaks characteristic of uranium oxide, whereas those of uranyl disappear completely. However, splitting peaks of UO_3 -520 at 25.9° and 33.9° indicate the formation of deoxidation products. Through combining with the results presented in Table 1, the optimum temperature of the reaction chamber in the flame denitrification reactor is determined to be in the range of 440–480 °C [22–24].

To elucidate the temperature-dependent valence change of U during uranyl nitrate thermal decomposition, X-ray photoelectron spectroscopy (XPS) is used to characterize the chemical state of U in the samples at different temperatures. Fig. 3 shows the high-resolution XPS spectra of U $4f_{7/2}$ orbitals under 0.2 MPa. The XPS peaks of UO₃-400, UO₃-440, and UO₃-480 show a single peak with a binding energy of 382.2 eV, confirming that the U in these samples exists entirely in the +6 valence state. The characteristic U $4f_{7/2}$ peak of UO₃-520 could be deconvoluted into two distinct peaks: One at 381.4 eV corresponding to U in the +5 valence state and another at 382.2 eV corresponding to U in the +6 valence state [25–27]. The proportions of the above valence states are summarized in Table S1.

In UO_3 -400, UO_3 -440, and UO_3 -480, the +6 valence state remains stable despite the high energy provided by alkane

combustion, which is sufficient to drive the reaction with no change in the uranium oxidation state. In addition, the oxygen in the combustion air effectively suppresses the reaction of U⁶⁺ to lower oxidation states, further confirming the feasibility of the flame denitrification reactor for producing UO₃. At 520 °C, a small amount of U⁵⁺ is formed accompanying with a slight decrease in the U 4f binding energy. However, this alternation in the U 4f binding energy is not conspicuous, indicating that uranium oxide at 520 °C exists in both the +5 and + 6 valence states. The XPS analysis reveals that progressive increase in U⁵⁺ and U⁴⁺ states contributes to gradual decrease in the U 4f binding energy during the transformation from UO₃ to U₃O₈. The above change is consistent with the established relationship between the average valence state of uranium in U₃O₈ and its lower oxidation state compared with UO₃. Further raising the reaction temperature promotes the conversion of uranyl nitrate into uranium oxide. However, an excessively high temperature leads to further deoxidation of UO₃ into U₃O₈ (Table 1); simultaneously, progressive darkening of sample colors with increasing temperature (Fig. S3) indicates partial conversion of UO₃ to U₃O₈ at 520 °C during flame denitrification.

Fig. 4 illustrates the Fourier-transform infrared (FTIR) spectra of four UO $_3$ products. The characteristic peak at 1500–1600 cm $^{-1}$ corresponds to asymmetric stretching vibrations of the nitrogen—oxygen double bond, whereas the peak at 1300–1390 cm $^{-1}$ is attributed to the asymmetric and symmetric stretching vibrations of the nitrogen—oxygen double bond. As the reaction chamber temperature increases, the intensities of these characteristic peaks gradually decrease, confirming that higher reaction temperature promotes the conversion of uranyl nitrate to uranium oxide. At temperature higher than 480 °C, uranyl nitrate is completely converted.

Scanning electron microscopy (SEM) images of the uranyl nitrate product reveal significant variations in crystal morphology, particle size, and porosity with increasing reaction temperature (Fig. 5). Small pores appeared on the surface of the uranyl nitrate decompose in the flame denitrification reactor, which is primarily attributed to the elevated temperature. Moreover, nitrogen oxides are gradually expelled from the uranyl nitrate sample during decomposition, and crystalline water is released as gaseous H2O, resulting in the formation of larger pores on the surface and inside the sample. A more detailed comparison of SEM images of the four samples indicates that with increasing reaction temperature, the degree of fragmentation is increased, which can be attributed to faster gas escape during decomposition that leads to the formation of smaller and denser pores with more severe sample fragmentation, thereby increasing the specific surface area of the obtained product. Compared with the UO₃ product prepared using a fluidized bed denitrification reactor (1–2 $m^2 \cdot g^{-1}$), the UO₃ product obtained from the flame denitrification reactor exhibits a significantly higher specific surface area of $11-13 \text{ m}^2 \cdot \text{g}^{-1}$. UO₃ particles with a larger specific surface area and higher reactivity are essential to meet the requirements of hydrogenation reduction, hydrofluorination, and fluorination in subsequent uranium enrichment stages [17,28,29].

Based on the position of the reduction peak in the hydrogen temperature-programmed reduction (H₂-TPR) spectrum, the temperature dependence of the redox performance of the uranium oxide samples is investigated. Fig. 6 shows the H₂-TPR spectra of the products under different atmospheres and temperatures. It is noted that the redox ability of uranium oxide is primarily determined by its reduction peak. For example, the reduction peak in the H₂-TPR curve of the four sample groups is mainly attributed to the reduction of high-to low-valence uranium. The large reduction peak exhibits a shoulder peak at lower temperatures, whereas the

low-temperature peak represents a reduction in surface-adsorbed oxygen ions by high-valence uranium, and the high-temperature peak represents the reduction in lattice oxygen ions by highvalence uranium [30]. In addition, as shown in Fig. 6, the temperature of the reduction peak first decreases and then increases. At reaction temperature of 400 °C, the reduction temperature increases due to the presence of some uranyl nitrate in the product. While the uranyl nitrate product is almost completely converted upon further increasing the reaction temperature so that the reduction of uranium oxide becomes increasingly difficult. Simultaneously, the reduction peak shifts to a higher temperature with the emergence of U⁵⁺, indicating that further reduction in the product becomes more difficult.

Flame denitration produces high-surface-area (11–13 $m^2 \cdot g^{-1}$), meeting nuclear fuel cycle requirements. This enhanced porosity results from explosive dehydration and decomposition of uranyl nitrate droplets in high-temperature flames, creating honeycomb-like pores via NO_x/H₂O release (Fig. 5); ultra-short residence time (<1 s) that enables kinetic "freezing" of submicron pores through rapid quenching; and steep thermal gradients that overcome conventional sintering limits through non-equilibrium processing. Additionally, while flame reactors maintain <50 kg·U inventory ($k_{\rm eff}$ < 0.90 at 1.5% enrichment), fluidized beds require >200 kg·U inventory, necessitating dual reactors at ≥ 5 tU·d⁻¹ throughput. However, the inevitable NO_x/CO₂ byproducts in flame denitration warrant future studies on adsorptive recovery technologies.

4. Conclusion

This study demonstrates a flame denitration strategy for synthesizing nuclear-grade UO₃ with controlled specific surface area $(11-13 \text{ m}^2 \cdot \text{g}^{-1}, \text{BET})$. Thermogravimetric analysis is employed to examine the thermal decomposition behavior of uranyl nitrate. Uranyl nitrate primarily undergoes dehydration from 0 °C to 200 °C, deoxidization from 200 °C to 267 °C, and denitrification from 268 °C to 300 °C. By contrast, maintaining the reaction chamber of the flame denitrification reactor between 440 °C and 480 °C results in high-quality UO₃ products. These products can be directly utilized in downstream processes, providing critical guidance for further advancements in nuclear fuel cycle systems.

CRediT Authorship Contribution Statement

Jiaxin Liu: Writing - original draft, Investigation, Funding acquisition, Formal analysis, Data curation, Conceptualization. Mingming Wu: Formal analysis, Data curation. Qichao Li: Investigation, Formal analysis. Rui Li: Formal analysis. Lei Li: Formal analysis, Data curation. Liudong Hou: Writing - original draft, Supervision, Funding acquisition, Yi Liu: Writing — review & editing, Supervision, Formal analysis. Jing Ma: Writing – original draft, Supervision, Funding acquisition.

Declaration of Competing Interest

The authors declare that they have no known competing financial interests or personal relationships that could have appeared to influence the work reported in this paper.

Acknowledgements

The authors are grateful to Xing Yuan Program of China National Nuclear Corporation (CNPE-8208) and National Natural Science Foundation of China (22478056) for the financial support.

Supplementary Material

Supplementary data to this article can be found online at https://doi.org/10.1016/j.cjche.2025.06.017.

References

- [1] J.X. Liu, S. Yang, Q.C. Li, L.M. Ji, X.F. Hou, L.D. Hou, J. Ma, Machine learning for forecasting factory concentrations of nitrogen oxides from univariate data exploiting trend attributes, Int. J. Adv. Nucl. React. Des. Technol. 6 (2) (2024)
- [2] J.X. Liu, Y. Tian, S. Yang, Y.Q. Qin, X.F. Hou, Y.T. Hu, L.D. Hou, J. Ma, Analysis of explosion incidents in nuclear fuel reprocessing facilities and recommendations for their prevention, Int. J. Adv. Nucl. React. Des. Technol. 6 (2) (2024) 108-116.
- [3] H.Y. Jeong, Y.I. Kim, Y.B. Lee, K.S. Ha, B.C. Won, D.U. Lee, D. Hahn, A 'must-go path' scenario for sustainable development and the role of nuclear energy in the 21st century, Energy Policy 38 (4) (2010) 1962-1968.
- [4] M.M. Wu, J.H. Yan, T.T. ji, K.P. Yu, Y.W. Sun, Y. Liu, X.G. Bai, Y.H. Liu, J.X. Liu, J. Ma, Y. Liu, Synthesis of (222)-oriented defect-rich MOF-808 membranes towards high-efficiency uranium rejection, J. Membr. Sci. 717 (2025) 123570.
- T. Mai, P. Denholm, P. Brown, W. Cole, E. Hale, P. Lamers, C. Murphy, M. Ruth, B. Sergi, D. Steinberg, S.F. Baldwin, Getting to 100%: six strategies for the challenging last 10%, Joule 6 (9) (2022) 1981-1994.
- [6] R. Busquim e Silva, M.S. Kazimi, P. Hejzlar, Nuclear fuel recycling: national and regional options for the US nuclear energy system, Energy Environ. Sci. 3
- [7] A.A. Adam, M.A.H. Eltayeb, O.B. Ibrahim, Uranium recovery from Uro area phosphate ore, Nuba Mountains, Sudan, Arab. J. Chem. 7 (5) (2014) 758-769.
- P. Goel, N. Choudhury, S.L. Chaplot, Atomistic modeling of the vibrational and thermodynamic properties of uranium dioxide, UO2, J. Nucl. Mater. 377 (3) (2008) 438 - 443.
- [9] S. Manna, S.K. Satpati, S.B. Roy, Development of a pneumatic transport system for bulk transfer of metal grade uranium oxide powder, Trans. Indian Ceram. Soc. 69 (2) (2010) 103-108.
- [10] B. Dussoubs, J. Jourde, F. Patisson, J.L. Houzelot, D. Ablitzer, Mathematical modelling of uranium dioxide conversion in a moving bed furnace, Powder Technol. 128 (2-3) (2002) 168-177.
- [11] M.H. Khani, H. Pahlavanzadeh, M. Ghannadi, Kinetics study of the fluorination of uranium tetrafluoride in a fluidized bed reactor, Ann. Nucl. Energy 35 (4) (2008) 704-707.
- [12] T. Kai, Theoretical research on gas-centrifugal separation for uranium enrichment, J. Nucl. Sci. Technol. 26 (1) (1989) 157–160.
- [13] R. Gupta, J. Gamare, S.K. Gupta, S.S. Kumar, Direct dissolution of uranium oxides in deep eutectic solvent: an insight using electrochemical and luminescence study, J. Mol. Struct. 1215 (2020) 128266.
- Y.C. Liu, Y.L. Liu, L. Wang, S.L. Jiang, Y.K. Zhong, Y.Z. Wu, M. Li, W.Q. Shi, Chemical species transformation during the dissolution process of U₃O₈ and UO₃ in the LiCl-KCl-AlCl₃ molten salt, *Inorg. Chem.* 61 (17) (2022) 6519–6529.
- [15] J. Zhang, L.H. Zhou, Z.M. Jia, X.F. Li, Y. Qi, C.T. Yang, X.H. Guo, S.Y. Chen, H.H. Long, L.J. Ma, Construction of covalent organic framework with unique double-ring pore for size-matching adsorption of uranium, Nanoscale 12 (47) (2020) 24044-24053.
- [16] V. Gonzalez, A.R. Otero, Formation of UO₃ particles in a fluidized bed, *Powder* Technol. 7 (3) (1973) 137-143.
- [17] W.H. Hedley, R.J. Roehrs, W.T. Trask Jr., Production of uranium dioxide by
- flame denitration, *Ind. Eng. Chem. Process Des. Dev.* 3 (1) (1964) 11–14. [18] D.J. Loaiza, W. Stratton, Criticality data for spherical ²³⁵U, ²³⁹Pu, and ²³⁷Np systems reflector-moderated by low capturing-moderator materials, Nucl. Technol. 146 (2) (2004) 143-154.
- [19] A. dos Santos, R. Fuga, R. Jerez, A.Y. Abe, E.A. Filho, A proposal for Benchmarking²³⁵U nuclear data, *Nucl. Sci. Eng.* 137 (1) (2001) 52–69.
- M.S. Dias, J.R.L. de Mattos, E.P. de Andrade, Very high burnup fuel for Angra 2 NPP within the 5 w/o limit of the ²³⁵U-enrichment, *Nucl. Eng. Des.* 346 (2019) 17–23.
- [21] W.H. Smith, Thermal dehydration of uranyl nitrate hydrates, J. Inorg. Nucl. Chem. 30 (7) (1968) 1761-1768.
- [22] E.J. Oerter, M. Singleton, Z.R. Dai, A. Deinhart, M. Thaw, M.L. Davisson, Hydrogen and oxygen stable isotope composition of water in metaschoepite mineralization on U₃O₈, Appl. Geochem. 112 (2020) 104469.
- [23] K.C. Shrivastava, G.P. Shelke, Nitrogen content determinations in different stages of thermal treatment involved in conversion of ammonium diuranate to uranium metal, J. Radioanal. Nucl. Chem. 314 (1) (2017) 105-110.
- [24] R. Eloirdi, D.H.M. Lin, K. Mayer, R. Caciuffo, T. Fanghänel, Investigation of ammonium diuranate calcination with high-temperature X-ray diffraction, J. Mater. Sci. 49 (24) (2014) 8436-8443.
- [25] N.L. Hansson, P.L. Tam, C. Ekberg, K. Spahiu, XPS study of external α-radiolytic oxidation of UO2 in the presence of argon or hydrogen, J. Nucl. Mater. 543 (2021) 152604.
- [26] K.O. Kvashnina, S.M. Butorin, P. Martin, P. Glatzel, Chemical state of complex uranium oxides, Phys. Rev. Lett. 111 (25) (2013) 253002.
- [27] G. Leinders, R. Bes, J. Pakarinen, K. Kvashnina, M. Verwerft, Evolution of the uranium chemical state in mixed-valence oxides, Inorg. Chem. 56 (12) (2017) 6784-6787.

- [28] M.R. Klosterman, E.J. Oerter, A.L. Deinhart, S. Chakraborty, M.J. Singleton, L. W. McDonald 4th, Oxygen kinetic isotope effects in the thermal decomposition and reduction of ammonium diuranate, ACS Omega 6 (45) (2021) 30856-30864.
- [29] N. Kumar, Y.R. Bamankar, K.T. Pillai, S.K. Mukerjee, V.N. Vaidya, V. Venugopal, Effect of feed solution composition and heat treatment conditions on the
- morphology of uranium oxide microspheres prepared by sol—gel process, *J. Nucl. Mater.* 359 (1–2) (2006) 80–92.

 [30] Y.Y. Dong, W.P. Liao, Z.H. Suo, Uranium oxide-supported gold catalyst for water—gas shift reaction, *Fuel Process. Technol.* 137 (2015) 164–169.